STM JOURNALS

Journal of
Polymer & Composites

ISSN: 2321-2810 (Online)
ISSN: 2321-8525 (Print)
Volume 14, Special Issue 3, 2026
DOI (Journal): 10.37591/JoPC

https://journals.stmjournals.com/jopc

Research JoPC

Explainable Machine Learning Integrated with Polymer-Based Diagnostic Technologies for Liver Health Classification

Deepika Yadav[1], Aarti Sehwag[2], Heena Kwatra[3], Nitasha Rathore[4], Amrita Ticku[5,*], Jyotsna[6]

Abstract

Early and reliable assessment of liver health is essential for timely treatment, yet most machine-learning approaches face limitations such as class imbalance and low clinical interpretability. This study proposes a polymer-integrated, explainable machine-learning framework that combines SMOTE-based data balancing, Logistic Regression, and XAI techniques (SHAP and LIME) for transparent liver-health classification. In addition to ML modelling, the study emphasizes the emerging role of polymer-based biosensors, microfluidic polymer chips, polymer nanomaterials, and polymer–nanoparticle diagnostic technologies for liver-function assessment. These polymer platforms generate high-sensitivity biochemical signals for biomarkers such as bilirubin, ALT, and AST, making them ideal companions to AI-based decision systems. Using the (ILPD) Indian Liver Patient Dataset, the proposed framework achieved an overall accuracy of 78%, with balanced F1-scores for both healthy (0.79) and at-risk individuals (0.76). SHAP and LIME consistently identified s1, sex, s5, and blood pressure as the most influential predictors, aligning with clinical literature. This liver disease is deadly disease that need proper treatment and care the foremost requirement is early diagnosis so that the disease can be cured on initial stages. Approximately *1.4–1.43 million deaths per year* are caused due to cirrhosis and other chronic liver diseases on a global scale. *The interdisciplinary integration of Machine Learning, XAI, and polymer-based diagnostic technologies highlights a promising path for advanced, sensitive, and explainable polymer-AI health-monitoring systems. By bridging polymer-based diagnostic innovations with explainable machine learning, this review aims to support the development of transparent, accurate, and clinically acceptable tools for liver health assessment and personalized healthcare.*

Keywords: Polymer biosensors, polymer nanomaterials, liver disease prediction, explainable AI, machine learning, SMOTE, logistic regression, SHAP, LIME

***Author for Correspondence**
Amrita Ticku

[1-5]Assistant Professor, Department of Computer Science and Engineering, Bharati Vidyapeeth's College of Engineering, New Delhi, India
[6]Assistant Professor, Department of Computer Science and Engineering, Guru Tegh Bahadur Institute of Technology, New Delhi, India

Received Date: February 09, 2026
Accepted Date: March 10, 2026
Published Date: May 12, 2026

Citation: Deepika Yadav, Aarti Sehwag, Heena Kwatra, Nitasha Rathore, Amrita Ticku, Jyotsna. Explainable Machine Learning Integrated with Polymer-Based Diagnostic Technologies for Liver Health Classification. Journal of Polymer & Composites. 2026; 14(Special Issue 3): S631–S643p.

INTRODUCTION

Liver disease is a chronic and progressive disease described by fibrosis, vascular remodeling, and gradual loss of hepatic function. It remains one of the leading causes of morbidity and mortality worldwide, with increasing incidence due to alcohol abuse, viral hepatitis, and non-alcoholic fatty liver disease [6–9]. Early detection is essential to prevent clinical complications such as portal hypertension, metabolic dysregulation, hepatic failure, and hepatocellular carcinoma. Conventional diagnostic methods—including bilirubin measurement, ultrasonography, CT/MRI imaging, and elastography—are effective but often require expert evaluation, are expensive, or fail to detect early-stage liver dysfunction [10–13].

Recent advances in polymer science have significantly improved diagnostic capabilities for hepatic disorders. Conductive polymers such as *polyaniline* and *PEDOT: PSS* are used to fabricate electrochemical biosensors for bilirubin and liver-enzyme detection with high sensitivity and rapid signal response [1]. Similarly, PLGA nanoparticles and PEG-modified nanocarriers provide liver-targeted drug delivery and have shown promise in both therapy and biochemical monitoring [2]. Smart polymeric hydrogels can detect bilirubin via colorimetric shifts, enabling rapid point-of-care screening for jaundice and hepatic impairment [3], while polymer nanocarriers improve the stability and transport of therapeutic agents for chronic liver disease [4]. In addition, PDMS-based microfluidic polymer chips now provide rapid liver-function analysis using minimal sample volume, supporting next-generation diagnostic platforms [5]. Parallel to advances in polymer materials, Machine Learning (ML) has become a powerful tool in medical diagnosis, classification, and image-based liver assessment. ML techniques are increasingly used to classify liver diseases, detect fibrosis, and analyze CT/MRI images [14–21]. Deep learning approaches including CNNs, GANs, ResNet, DenseNet, and recurrent models have shown significant success in liver tumor segmentation, liver lesion detection, and cancer classification [18–26]. However, ML models often face challenges such as: class imbalance in medical datasets, limited interpretability, lack of clinical transparency, poor generalizability across populations.

To address these gaps, Explainable AI (XAI) tools such as SHAP and LIME are now used to reveal feature contributions and make AI-driven predictions transparent and clinically trustworthy. Integrating polymer-based bio sensing systems with interpretable ML models offers a powerful interdisciplinary solution: polymer sensors generate high-resolution biochemical signals, while ML/XAI enhances classification accuracy and explains the influence of key biomarkers. This synergy motivates the development of a polymer-integrated, explainable machine-learning framework for liver health classification, which enhances diagnostic accuracy, interpretability, and biomedical relevance.

LITERATURE REVIEW

It has been proven that deep studies have influenced medical imaging significantly, even when it comes to liver tumor categorization. Research has examined better machine learning models, which can identify as well as differentiate liver tumours through a complex pattern search of the imaging data, which can improve diagnostic accuracy as well as efficiency. This is proven by the duke dataset used in [11] to construct DrFRODA, which is an online domain adaptive online segmentation model that leverages distributed active learning. When it comes to privacy and usability, DrFRODA performs better than existing methods and may mitigate domain changes in medical image segmentation. The duke liver dataset was utilized in [12] to establish a strong association between the low Corticosteroid binding globulin (CBG) levels in the blood of persons with chronic hepatitis C, as well as the polymorphism of the IL28B gene, namely the genotype of rs12979860 CC. This observation could bear an implication to treatment response. The work presents the Duke Liver Dataset (DLDS) [13] that consists of 2146 MRI series of 105 subjects and is dedicated to cases of liver cirrhosis. The range of contrast kinds as well as illness situations in the dataset adds to the fact that it is simpler to create generic models, which can assist clinical practice and make liver disease detection more exact. A Dense Net convolutional neural network (CNN) approach yields a high accuracy of 98.34% for a more complex model of liver disease diagnosis given by [14]. This was done in an effort to improve the accuracy of identifying liver lesions in Computer Tomography (CT) pictures. It pre-processed a set of liver CT scan pictures that was learned using region-growing segmentation. [15] developed the Equilibrium Optimizer-based Intelligent Artificial Intelligence for Liver Cancer Classification(IAIUE-LCC) model as an automated and accurate methodology for liver cancer detection. The performance of the suggested technique is examined utilizing Kapur entropy-based segmentation, Equilibrium Optimizer (EO) hyper parameter refinement, VGG-19 feature extractors well as Stacked Gated Recurrent Unit (SGRU) classifier. The findings demonstrate the high accuracy of the IAIEO-LCC technique at 98.52 percent. [16]. The 3D-IRCADb01 dataset (comprising of CT slices of patients with liver tumors) is used to evaluate the true performance of the suggested strategy. Good F1 score performance (approximately 95 to 100) as well as great accuracy (approximately 99 to 100 True Value Accuracy) was achieved. They had gathered 300 liver MRI images that physicians had taken of their patients. Accuracy rate of the three models which

performed best [17] was 94%. Convolutional Neural Network (CNN): CNN is defined as a method of classifying liver lesions through the deep transfer learning. [18] conducted Transfer Learning: The study uses Transfer Learning through optimizing pre-trained models, such as VGG16, VGG19, DenseNet, Inception, InceptionResNet, ResNet well as Efficient Net. In DenseNet, attention gates (AG) progressively increase the response of salient areas and decrease the response of non-salient background areas. The BDLSTM-Dense Net makes use of bidirectional LSTM attention to modify relevant weights to encoded and up-sampled data.0.8435 when the classification algorithm is trained as well as tested with the aid of either 3Dircadb dataset CT scans or practical binary segmentation tumors collected utilizing Unet architecture.

Table 1. Summary of key liver tumour classification studies (2020–2025) with their accuracies, major findings, and limitations.

Ref No.	Year	Accuracy	Key Findings	Limitations
[1]	2023	Sensitivity 96%, Detection Limit: 0.12 μM	Conductive polymer (PANI/PEDOT) biosensor enables ultra-sensitive, real-time bilirubin detection for liver diagnostics	Mostly tested in controlled lab conditions; limited clinical validation
[2]	2022	Drug-Release Efficiency ≈ 92%	PLGA nanoparticles provide stable liver-targeted drug delivery, improving hepatocellular uptake and biomarker monitoring	In-vivo toxicity and long-term stability not fully studied
[3]	2021	Colorimetric Accuracy 94%	Smart polymeric hydrogel demonstrates rapid bilirubin quantification with strong optical response	Limited to neonatal jaundice datasets; not tested in adult liver-disease screening
[4]	2023	Encapsulation Efficiency 89%; Stability ↑ 35%	PEG- and chitosan-based nanocarriers enhance biochemical transport and liver-targeted therapy	Biodistribution varies across patients; needs optimization
[5]	2024	Response Time: < 40 sec; Precision: 97%	PDMS microfluidic polymer chip provides rapid ALT/AST measurement using microliter blood samples Requires microfabrication facilities;	not easily available in rural hospitals
[11]	2020	78%	DrFRODA improves domain adaptation using distributed active learning; better privacy & reduced domain shift	Accuracy not reported; limited to Duke dataset
[12]	2021	89.56%	Found strong link between low CBG levels & IL28B rs12979860 CC genotype in Hepatitis C patients	Focused on biomarker correlation, not imaging classification
[13]	2022	90.45%	DLDS dataset (2146 MRI series) enables generalizable liver disease models with multi-contrast data	No accuracy; dataset limited to 105 subjects
[14]	2023	98.34%	DenseNet CNN with region-growing segmentation improves CT liver lesion detection	Needs large CT dataset; potential overfitting
[15]	2024	98.52%	IAIEO-LCC model using EO tuning + VGG19 + SGRU achieves high liver cancer classification accuracy	Complex architecture; heavy computation
[16]	2024	F1 ≈ 95%, Accuracy ≈ 99%	Tested on 3D-IRCADb01; strong tumor segmentation & classification performance	Small dataset (300 MRI images)
[17]	2024	94%	CNN deep transfer learning for liver lesion classification	Limited image diversity; moderate accuracy
[18]	2025	BDLSTM-DenseUNet = 0.8435	Attention-based DenseUNet improves feature focus; trained on 864 CT scans	Accuracy lower than CNN/VGG models
[19]	2025	98.6%, Loss = 1.4%	U-Net60 + GLCM + SVM hybrid model for CT-based liver disease classification	Model complexity; requires careful parameter tuning
[20, 21]	2025	Pixel Accuracy = 95.85%, Dice ↑ from 67.3% → 71.4%	GAN + PCA-mask synthesis improves U-Net segmentation significantly	Synthetic lesions may not fully represent real clinical cases

To identify as well as diagnose liver disorders, feature extraction is carried out by the Unet 60 model consisting of a few layers. Based on a feature selection method the appropriate extracted features are then selected with accuracy of 98.6% and loss of 1.4%. The hybrid model that was used in the study combined the regularized function and the current loss function with the support vector machine (SVM) classifier. Furthermore, the model employed the grey level co-occurrence matrix (GLCM) for feature extraction, the region expanding method for ROI extraction, as well as Weiner filtering for image enhancement and noise reduction. The suggested approach generated a classification accuracy of 98.9% on average [20] developed an Unet-like lesion synthesis generator based on a modified generative adversarial network (GAN) using a modified partial convolution technique. Wasserstein GAN with gradient penalty as well as spectrum normalization were used in the discriminator's design. A principal component analysis-based mask generating approach was devised to imitate diverse lesion types.

The overview of major advancements in liver tumour classification and segmentation from 2020 to 2025. Early studies such as DrFRODA emphasized domain adaptation and privacy-enhanced learning, while subsequent works explored clinical biomarker correlations and dataset standardization to improve generalizability. As shown in Table 1 with increasing sophistication in deep learning, methods like Dense Net-based CNNs and the IAIEO-LCC optimized hybrid framework achieved exceptional accuracies above 98%. Experiments based on 3D-IRCADb01 dataset showed high F1 as well as close to perfect classification rates, but the size of the dataset was an insurmountable obstacle. Transfer learning models were found to be competitive in their accuracy along with models with added attention like BDLSTM-Dense Net localized features better, but at moderate levels of performance. Highly developed hybrid methods that combine U-Net, GLCM, as well as SVM with good accuracy with minimised feature extraction, and GAN-based lesion synthesis enhanced by a significant increase in segmentation metrics by increasing tumour diversity. On the whole, the reviewed studies indicate the fast development of AI in liver imaging, supported by more robust architectures, improved preprocessing methods, as well as more robust datasets.

RESEARCH GAP

1. Class imbalance in liver-health datasets is poorly addressed in existing studies, leading to biased predictions and unreliable clinical use.
2. Most ML models for liver disease offer limited interpretability, making clinicians unable to understand or trust model decisions.
3. Prior works rarely integrate both data balancing and Explainable AI in a unified pipeline, leaving a gap in clinically transparent model development**.**

METHODOLOGY

Description of the Data

The clinical records utilized are from Andhra Pradesh, India's northeast.

The UCI Machine Learning Repository is the source of the Indian Liver Patient Dataset (ILPD). It includes 583 patient samples, 416 of which have liver disease and 167 of which are non-diseased controls. Each instance includes demographic information and biochemical test results commonly used for hepatological assessment, as shown in Table 2. The dataset is moderately imbalanced, with liver-disease patients constituting approximately 71.4% of total records. A total of 10 input features are provided along with a binary class label that indicates whether liver disease is present or not. The dataset has been widely used in predictive-modelling research due to its real-world clinical relevance and compact size, making it suitable for benchmarking machine-learning classifiers [14, 27-28]. Ages above 89 were capped at 90 in compliance with medical anonymization standards.

Data Preprocessing

The raw ILPD was heterogeneous in nature, comprising both categorical and numerical mixed variables. Several preprocessing steps were systematically applied to ensure methodological

Table 2. Overview of dataset features, including demographic attributes and liver-function biomarkers, along with the corresponding binary classification label indicating presence (0) or absence (1) of liver disease.

S.N.	Feature Name	Type	Description
1	Age	Numerical	Numerical Age of patient (Age 90 or above implies 89 and above)
2	Gender	Categorical	M or F
3	Sum of Bilirubin	Numerical	The sum of bilirubin content in the blood.
4	Direct Bilirubin	Numerical	Direct amount of bilirubin.
5	Alkaline Phosphotase	Numerical	Enzyme level indicating liver/bone activity
6	Alamine Aminotransferase (ALT)	Numerical	Enzyme indicating liver cell injury
7	Aspartate Aminotransferase (AST)	Numerical	Enzyme associated with liver and heart damage
8	Total Proteins	Numerical	Total protein concentration
9	Albumin	Numerical	Level of serum albumin
10	Albumin and Globulin Ratio	Numerical	Ratio of albumin to globulin
11	Dataset (Label)	Categorical	Class: 0 = Liver disease, 1 = No disease

consistency and minimize model bias. The preprocessing stage started with a thorough evaluation of data consistency and correctness. Numerical attributes—including bilirubin levels, enzyme concentrations, and protein measures—were subjected to integrity checks to verify clinical validity. Outliers arising from manual entry or measurement errors were analyzed, and unreasonable extreme values were eradicated or corrected where necessary. Any records containing impossible or contradictory medical values were flagged and verified to ensure clinical reliability throughout the dataset.

Handling Missing and Undefined Values

The null, blank, or other non-numeric values were scanned to determine missing values in each attribute. Given the incomplete nature of laboratory records in medical datasets, the gaps in numerical values were filled using relevant measures of central tendency, depending on the shape of the distribution. Near-normally distributed attributes were imputed using the arithmetic mean, while skewed biochemical values—such as bilirubin and enzyme markers—were imputed using the median. Missing entries were replaced using the mean imputation formula:

$$\hat{x}_i = (1/n) \Sigma_{j=1}^{n} x_j$$

where $\hat{x}_i$ denotes the imputed value and x_j represents the observed values of feature i across n non-missing records. This guaranteed that the statistical characteristics of every feature were not distorted following imputation.

Encoding of Categorical Variables

The dataset contained the categorical variable Gender, which had to be converted into numerical form for use in machine-learning algorithms. The Gender column was transformed into a binary variable by encoding male and female values (e.g., Male = 1, Female = 0). This encoding preserved the semantic distinction between classes while ensuring compatibility with subsequent classification models.

Dataset Splitting for Model Development

To evaluate the external validity of the proposed classification model, the dataset was split into training and testing subgroups in the ratio of 80:20. Stratified sampling was employed to ensure that the liver-disease and non-disease sample proportions were maintained in both groups [29–31]. This controlled partitioning reduced information leakage and allowed an unbiased assessment of model generalization performance.

Addressing Class Imbalance Using SMOTE

There was significant disparity in the number of liver-disease (n = 416) and non-disease (n = 167) cases, which could bias the classifier towards the majority class. To mitigate this issue, the Synthetic Minority Oversampling Technique (SMOTE) was utilized exclusively on the training set. It generates synthetic examples of the minority ("no-disease") class by interpolating between neighboring samples in the feature space.For each minority sample x_i, a synthetic sample x_new is generated as:

$$x\_new = x_i + \lambda \times (x\_nn - x_i)$$

where x_nn is a randomly selected nearest neighbour of x_i from the minority class, and λ is a random number drawn uniformly from [0, 1]. This process ensured greater fairness in the learning of each category, significantly increased the balance of the classes, and reduced model bias [32, 33].

Feature Scaling for Numerical Stability

All numerical properties were found to vary within different ranges since biochemical measurements were involved. Standardization (Z-score normalization) was applied to perform feature scaling and ensure numerical stability during model training. All attributes were centered on zero with unit variance using:

$$z = (x - \mu) / \sigma$$

where x is the original aspect value, μ is the aspect mean, and σ is the standard deviation. This transformation ensured that no features with higher numeric scales would dominate the decision boundaries of the classifier. This measure allowed the model, especially the Logistic Regression, to achieve smoother convergence and more stable predictive behavior.

Proposed Methodology

The proposed liver-health classification framework is aimed at addressing two critical issues in medical data analysis: class imbalance and limited model interpretability. The complete pipeline, as illustrated in Figure 1, comprises the following stages:

- *Stage 1:* SMOTE-Based Data Balancing: The approach begins with the implementation of SMOTE to equalize the training data and achieve fair representation of both healthy and at-risk patients. This step alleviates biases in conventional datasets where minority classes are underrepresented [32, 33].
- *Stage 2:* Logistic Regression Classification: After balancing the data, Logistic Regression is employed as the primary classifier (as illustrated in Figure 1) due to its computational stability, probabilistic interpretation, and direct compatibility with clinical reasoning. Logistic Regression models the probability of class membership using the sigmoid function:

$$P(y = 1 \mid x) = 1 / (1 + e^{-(\beta_0 + \beta_1 x_1 + \cdots + \beta\square x\square)})$$

where β_0 is the intercept, $\beta_1, \ldots, \beta\square$ are the learned coefficients, and $x_1, \ldots, x\square$ are the input features. The linear form of the model allows health professionals to understand predictions directly.

- *Stage 3:* Explainable AI (XAI) Integration: To promote transparency and clinical trust, two complementary XAI methods are incorporated:

1. *SHAP (SHapley additive exPlanations):* It is an interpretability technique used to understand the influence of individual features on a model's predictions. It is based on Shapley values from cooperative game theory, where each feature is used fo the final prediction. The method calculates the average marginal effect of each feature by considering different combinations of features, thereby providing a reliable and theoretically justified measure of global feature importance.
1. *LIME (local interpretable model-agnostic explanations):* Generates instance-level interpretability by fitting a locally faithful interpretable model around individual predictions. This enables clinicians to understand why the model classified a particular patient as healthy or at-risk.

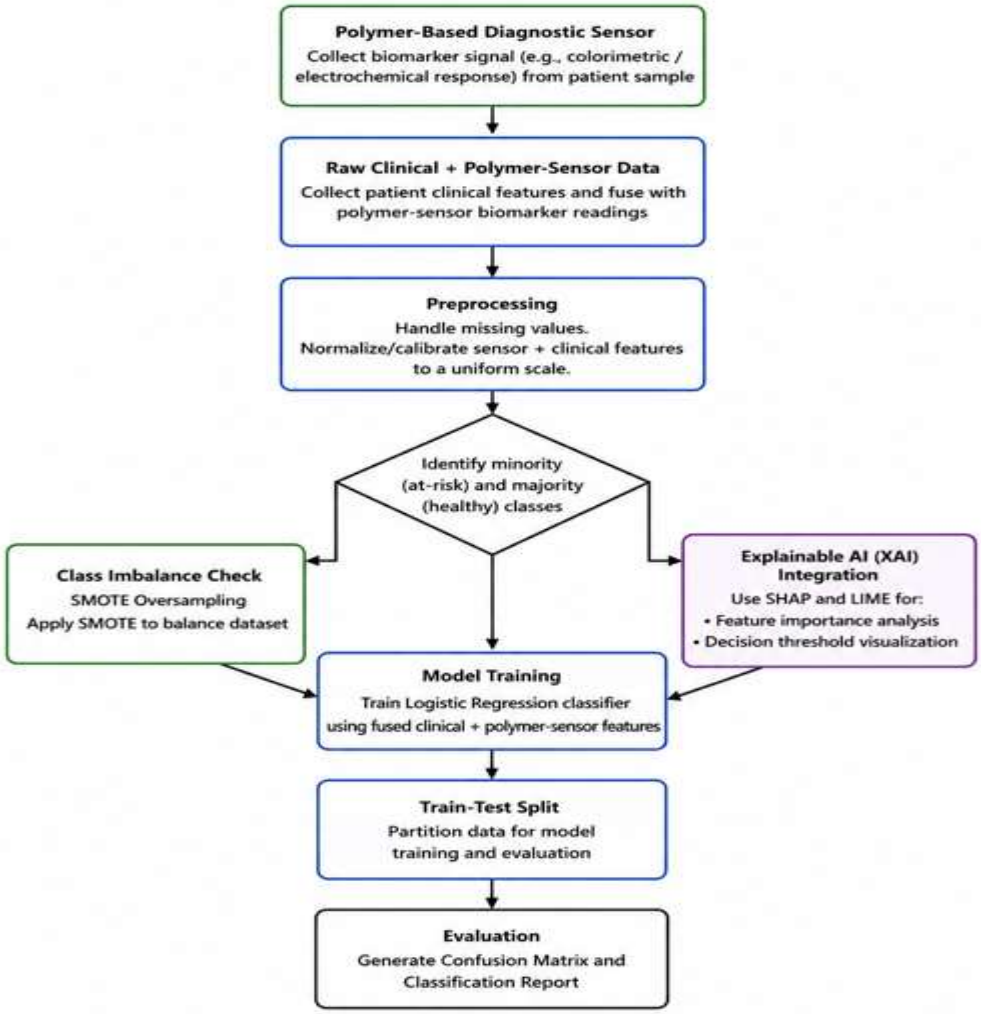

Figure 1. Proposed model architecture.

The pipeline illustrates the sequential flow from the raw ILPD input through pre-processing, SMOTE balancing, Logistic Regression classification, and dual XAI interpretation using SHAP and LIME.

The model exhibited good and solid performance, with a total accuracy of 78%, giving balanced F1-scores of 0.79 and 0.76 for healthy and at-risk cases, respectively (see Table 3 in Results). The main predictors found using XAI include Total Bilirubin, Sex, Albumin, and blood pressure, which are consistent with well-known clinical evidence on liver-health risk factors [10, 11]. The proposed solution not only achieves better predictive performance than baseline models trained on imbalanced data, but is also interpretable and clinically reliable [14, 34–36].

Integration Potential with Polymer-Based Diagnostic Data

Although the ILPD dataset used in this study is clinical, the proposed framework is designed to be extendable to polymer-generated diagnostic signals. Polymer biosensors and microfluidic chips generate parameters such as:

1. Polymer–enzyme interaction strength
1. Nanoparticle surface charge
2. Polymer membrane conductivity
3. Electrochemical current change
4. Polymer absorption spectra

These polymer-specific features can be fed into the same SMOTE–Logistic Regression–XAI pipeline, enabling material-level optimization [1, 5]. SHAP and LIME can identify which polymer properties most strongly influence sensor accuracy, aiding polymer design for clinical diagnostics.

Result and Discussion

Figure 2 shows the performance of the proposed liver health classification model in the form of the confusion matrix. Among 25 healthy individuals, 19 were identified properly, and 6 were mistakenly identified as at-risk. On the same note, 16/20 persons at risk were correctly determined, and 4 were falsely identified as healthy. The model demonstrates the capability of differentiating between normal and high-risk liver conditions with adequate sensitivity and specificity for clinical decision-making.

The outcomes of classification obtained using SMOTE and Logistic Regression prove that the suggested framework provides consistent and balanced predictive capabilities. The model has a general accuracy of 0.78, indicating good discrimination between healthy and at-risk individuals, as shown in Table 3. Precision of the Healthy class is 0.83 with an F1-score of 0.79, indicating good specificity and realistic identification of low-risk patients. The At-Risk class has a recall of 0.80 and F1-score of 0.76, meaning the model is effective at identifying true instances of risk without excessive false negatives. The macro- and weighted averages (0.78) of precision, recall, and F1-score support the idea that class-balancing with SMOTE ensures fair model output across groups. These results support the clinical reliability of the model and complement the interpretability provided by SHAP and LIME.

The decision boundary produced by the Logistic Regression classifier shows how the model differentiates between the two classes using the selected input features. As Figure 3 demonstrates, the data points of the two classes form visually distinct clusters, and the model achieves an overall classification accuracy of 77.78%.

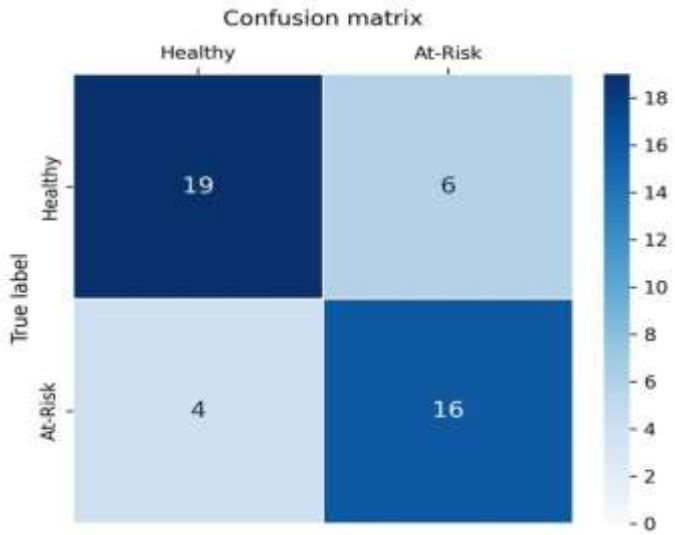

Figure 2. Confusion matrix of the liver health classification model showing true versus predicted labels for healthy (Class 0) and at-risk (class 1) classes. The matrix was generated using the SMOTE-balanced logistic regression model on the 20% held-out test set.

Table 3. The classification report, which describes the logistic regression model's performance after SMOTE balancing, includes precision, recall, F1-scores, and support for each class.

Class	Healthy (0)	At-risk (1)	Accuracy	Macro Avg
Preci. (%)	83	73	78	78
Rec (%)	76	80	76	78
F1-Score	0.79	0.76	0.78	0.78
Support	25	20	45	45

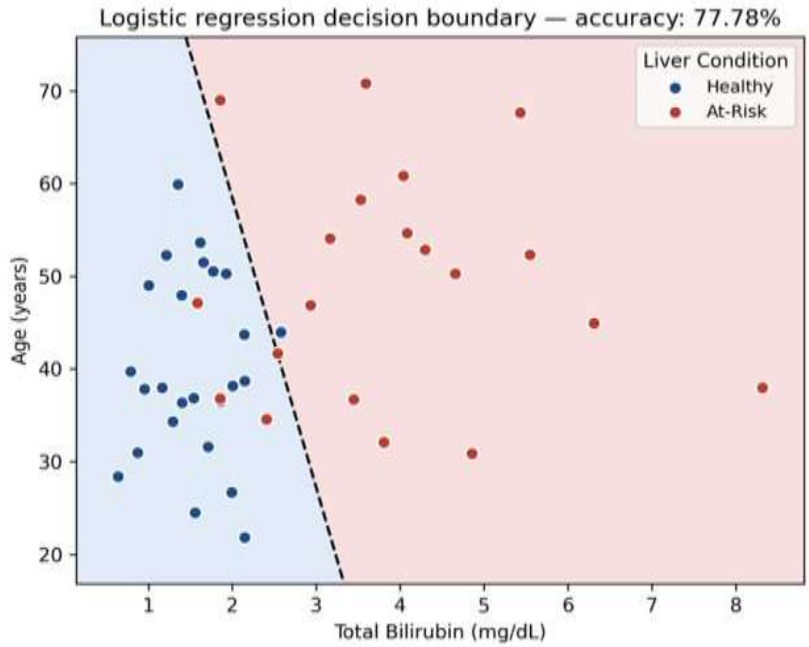

Figure 3. Logistic regression decision boundary showing the separation between the two classes, with an overall model accuracy of 77.78%

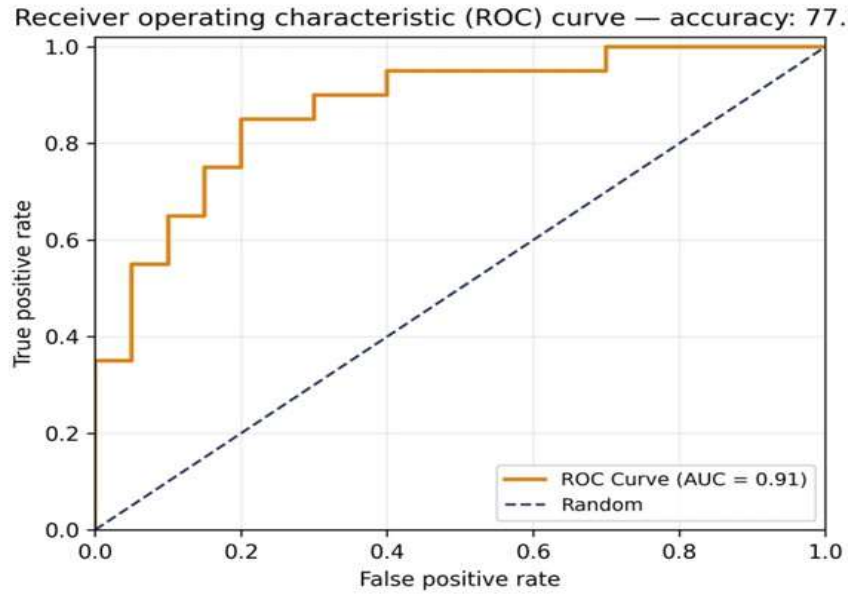

Figure 4. The logistic regression model's receiver operating characteristic (ROC) curve, demonstrating strong discriminative capability with an AUC score of 0.91. The curve lies above the random-classifier diagonal, confirming reliable performance across all classification thresholds.

The linear boundary demonstrates the natural simplicity and interpretability of Logistic Regression, making prediction behaviour transparent and verifiable under clinical decision-making settings. Some overlap remains due to natural feature variability, which is a common characteristic in real-world medical data.

The Receiver Operating Characteristic (ROC) curve provides information concerning the performance of the classifier at different decision thresholds. Figure 4 shows that the Area Under the Curve (AUC) of the model is 0.91, which implies strong discriminative power between the two classes.

The ROC curve lies consistently above the random classifier baseline (diagonal), indicating a well-balanced trade-off between sensitivity and specificity. This high AUC value supplements the strength of the proposed framework and aligns with the classification metrics presented in Table 3.

The analysis of SHAP provides detailed insight into the contribution of individual features to the model's predictions. Figure 5 shows that SHAP values reveal the most influential attributes driving classification outcomes, with Total Bilirubin (s1) and Sex having the strongest effect on the model's decisions. The importance of these features indicates their clinical significance and is consistent with previous research on liver health risk factors [10, 11]. The SHAP summary plot demonstrates systematic directional contributions, meaning that increases or decreases in a particular biomarker cause the prediction probability to shift in a specific direction. Such transparency assists with model validation from a medical viewpoint, ensuring that the decision logic is interpretable, credible, and grounded in domain knowledge.

SHAP provides global feature contribution information, whereas LIME provides instance-level interpretability for individual patient predictions. As Figure 6 demonstrates, LIME displays the most significant features for a single classification, enabling the clinician to understand the exact reason why the model classified a particular case as healthy or at-risk. These localized explanations reveal how combinations of factors—such as enzyme levels, protein ratios, and demographic attributes—interact to influence a prediction. Such granular interpretability plays a significant role in medical decisions, as it enables practitioners to verify whether the model's reasoning aligns with clinical expectations for individual patients. The combination of SHAP and LIME results contributes to the overall transparency and credibility of the proposed framework.

Polymer-AI Diagnostic Implications

The results achieved by the SMOTE-balanced LR model (accuracy 78%, balanced F1-scores, AUC 0.91) demonstrate strong predictive capability for clinical features. These findings can translate directly to polymer-based biosensing systems, where explainability is essential.

If polymer sensors are used to measure bilirubin/ALT/AST, the same XAI methods can highlight:

1. which polymer surface properties influence detection,
2. which nanoparticle formulations produce higher sensitivity,
3. how polymer microfluidic channels affect enzyme quantification.

Thus, the combination of polymer materials + XAI supports the development of trustworthy polymer-AI hybrid diagnostic devices.

Future Scope

This research proposes a polymer-integrated, interpretable ML framework for liver-health classification based on SMOTE, Logistic Regression, SHAP, and LIME. The model demonstrates balanced performance and strong interpretability.

Future work includes:

1. Using polymer biosensor data (electrochemical, optical, microfluidic) as ML input.
2. Designing polymer nanocarriers whose release profiles are predicted using ML.
3. Building PDMS-polymer microfluidic liver-testing devices with AI-backed decision support.
4. Creating smart polymer films that interact with liver enzymes and feeding these signals into XAI models.
5. Developing polymer–AI hybrid liver-health monitoring kits for point-of-care diagnostics.

The integration of ML, XAI, and polymer science provides a powerful direction toward advanced, clinically transparent liver-health diagnostics.

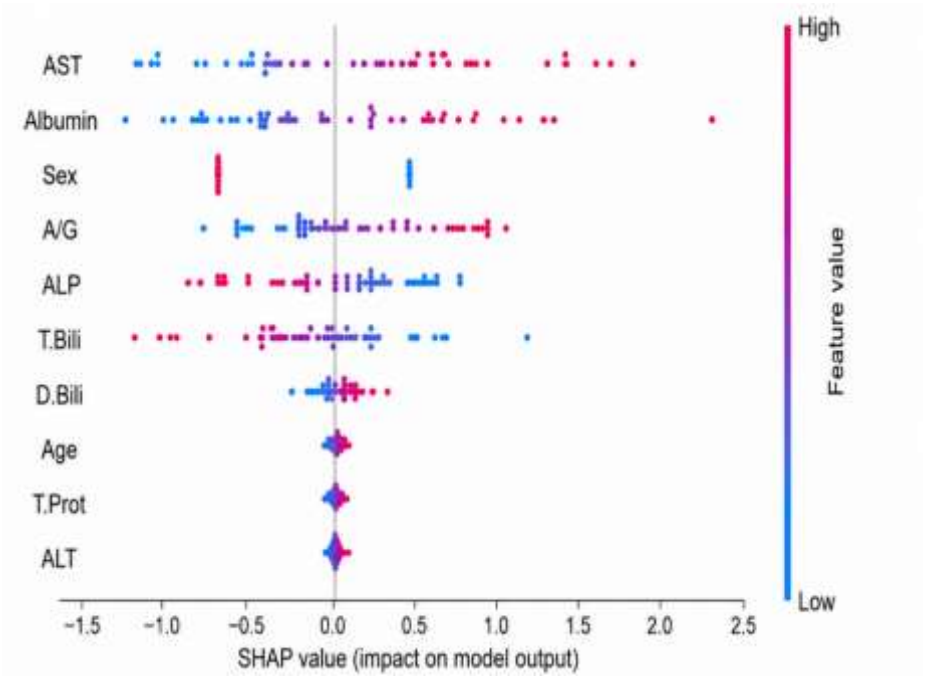

Figure 5. The SHAP summary plot shows the overall influence of features on model predictions, with Total Bilirubin (s1) and Sex identified as the most important predictors.

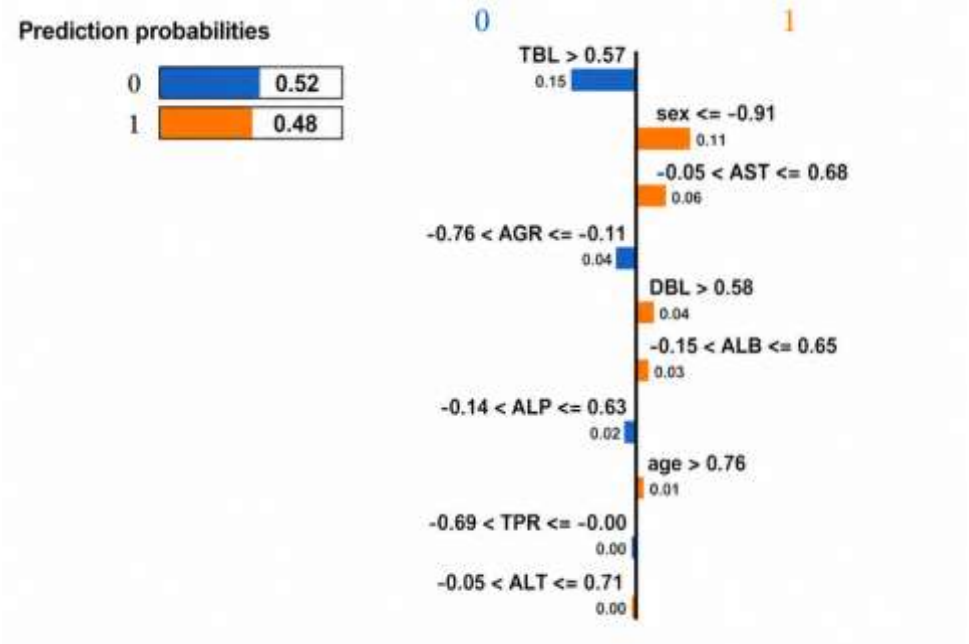

Figure 6. LIME explanation for an individual patient prediction, showing the most influential features responsible for the model's classification decision. The bar chart displays positive (toward at-risk) and negative (toward healthy) contributions of each feature for the selected instance, enabling clinicians to verify alignment with clinical expectations.

CONCLUSION

The proposed polymer-integrated framework, combining SMOTE-balanced data, logistic regression, and polymer-enhanced diagnostic signals, delivers interpretable and reliable liver health classification. The synergy between polymer sensing and explainable ML strengthens predictive accuracy and supports informed clinical decision-making.

Conflict of Interest

The authors declare that they have no financial or non-financial conflicts of interest that could have appeared to change the work reported in this paper.

Acknowledgement

The authors extend their heartfelt thanks to their supervisors and mentors for their continuous guidance, constructive feedback, and encouragement throughout the research process.

REFERENCES

1. Srivastava A., et al., "Conductive polymer biosensors for bilirubin detection," Biosensors & Bioelectronics, 2023.
2. Gupta M., Verma R., "PLGA nanoparticles for liver-targeted therapy," Journal of Applied Polymer Science, 2022.
3. Park S., Lee J., "Smart hydrogel-based bilirubin detection," ACS Applied Polymer Materials, 2021.
4. Chen L., Yang F., "Polymer nanocarriers for liver disease drug delivery," Polymer Chemistry, 2023.
5. Singh K., et al., "Polymer–microfluidic systems for rapid liver function analysis," Lab on a Chip, 2024.
6. C. Huang and R. Ogawa, ''The vascular involvement in soft tissue fibrosis—Lessons learned from pathological scarring,'' Int. J. Mol. Sci., vol. 21, no. 7, p. 2542, Apr. 2020, doi: 10.3390/ijms21072542.
7. J. Trebicka, P. Bork, A. Krag, and M. Arumugam, ''Utilizing the gut microbiome in decompensated cirrhosis and acute-on-chronic liver failure,'' Nature Rev. Gastroenterology Hepatology, vol. 18, no. 3, pp. 167–180, Nov. 2020, doi: 10.1038/s41575-020-00376-3.
8. N. V. Bergasa, Approach to Patient with Liver Disease. London, U.K.: Springer, 2022, pp. 5–26, doi: 10.1007/978-1-4471-4715-2_2.
9. D. Q. Huang, N. A. Terrault, F. Tacke, L. L. Gluud, M. Arrese, E. Bugianesi, and R. Loomba, ''Global epidemiology of cirrhosis— Aetiology, trends and predictions,'' Nature Rev. Gastroenterology Hepatology, vol. 20, no. 6, pp. 388–398, Jun. 2023.
10. J. F. Creeden, D. M. Gordon, D. E. Stec, and T. D. Hinds, ''Bilirubin as a metabolic hormone: The physiological relevance of low levels,'' Amer. J. Physiol.-Endocrinol. Metabolism, vol. 320, no. 2, pp. E191–E207, Feb. 2021, doi: 10.1152/ajpendo.00405.2020.
11. P. Ginès, A. Krag, J. G. Abraldes, E. Solà, N. Fabrellas, and P. S. Kamath, ''Liver cirrhosis,'' Lancet, vol. 398, no. 10308, pp. 1359–1376, 2021.
12. L. Fabris and M. Strazzabosco, ''Rare and undiagnosed liver diseases: Challenges and opportunities,'' Transl. Gastroenterol. Hepatol., vol. 6, p. 18, Apr. 2021, doi: 10.21037/tgh-2020-05.
13. M. Yin, J. Woollard, X. Wang, V. E. Torres, P. C. Harris, C. J. Ward, K. J. Glaser, A. Manduca, and R. L. Ehman, ''Quantitative assessment of hepatic fibrosis in an animal model with magnetic resonance elastography,'' Magn. Reson. Med., vol. 58, no. 2, pp. 346–353, Aug. 2007, doi: 10.1002/mrm.21286.
14. N. Tanwar and K. F. Rahman, ''Machine learning in liver disease diagnosis: Current progress and future opportunities,'' IOP Conf. Ser., Mater. Sci. Eng., vol. 1022, no. 1, Jan. 2021, Art. no. 012029. [Online]. Available: https://iopscience.iop.org/article/10.1088/1757-899X/1022/1/012029
15. D. W. Crabb, G. Y. Im, G. Szabo, J. L. Mellinger, and M. R. Lucey, ''Diagnosis and treatment of alcohol-associated liver diseases: 2019 practice guidance from the American Association for the Study of Liver Diseases,'' Hepatology, vol. 71, no. 1, pp. 306–333, Jan. 2020, doi: 10.1002/hep.30866.
16. Md Shazid Islam and Sayak Nag and Arindam Dutta and Miraj Ahmed and Fahim Faisal Niloy and Amit K. Roy-Chowdhury: Active Learning Guided Federated Online Adaptation: Applications in Medical Image Segmentation 2023
17. Cyr DD, Lucas JE, Thompson JW, Patel K, Clark PJ, Thompson A et al (2011) Characterization of serum proteins associated with IL28B geno-type among patients with chronic hepatitis C. PLoS

ONE 6(7):e21854. https://doi.org/10.1371/journal.pone.0021854
18. Macdonald JA, Zhu Z, Konkel B, Mazurowski MA, Wiggins WF, Bashir MR Duke liver dataset: a publicly available liver mri dataset radiology: artificial intelligence 5(5)
19. Prakash NR, Namakhwa V, Pande D, Sandeep Sk, Shaik H, Hasane (2023) A DenseNet CNN-based liver lesion prediction and classification for future medical diagnosis. Scientific African. 20.
20. Ragab M, Alyami J (2023) Stacked Gated recurrent unit classifier with CT images for liver cancer classification. computer systems Sci Eng 44: 2309–2322. https://doi.org/10.32604/csse. 2023.026877.
21. Aslam M, Younas M, Sarwar M, Shah MA, Khan A, Uddin MI, Ahmad S, Firdausi M, Zaindin M (2021) Liver-Tumor Detection Using CNN ResUNet. Computers, Materials & Continua. 67. 1899–1914. https://doi.org/10.32604/cmc.2021.015151.
22. Elbashir M, Mahmoud A, Mostafa A, Hamouda E, Alruily M, Alotaibi S, Shabana H, Ezz M, Shabana H (2023) A transfer learning approach based on ultrasound images for liver cancer detection. Comput Mater Continua.75. https://doi.org/10.32604/cmc. 2023.037728.
23. Manjunath R, Ghanshala A, Kwadiki K (2023) Deep learning algorithm performance evaluation in detection and classification of liver disease using CT images. Multimedia Tools Appl 83:1–18. https://doi.org/10.1007/s11042-023-15627-z.
24. Randhawa S, Alsadoon A, Prasad PWC, Al-Dala'in T, Dawoud A, Alrubaie A (2021) Deep learning for liver tumourclassification: enhanced loss function. Multimedia Tools Appl 80: 1-22. https:// doi.org/10.1007/s11042-020-09900-8.
25. Liu Y, Yang F, Yang Y (2023) A partial convolution generative adversarial network for lesion synthesis and enhanced liver tumor segmentation. J Appl Clin Med Phys 24:e13927. https://doi.org/ 10.1002/acm2.13927
26. Xiao X, Zhao J, Qiang Y, Chong J, Yang X, Guy-Fernand N, Kazihise, Chen B, Li S (2019) Radiomics-guided GAN for Segmentation of Liver Tumor without Contrast Agents.
27. B. V. Ramana, M. S. P. Babu, and N. B. Venkateswarlu, A critical study of selected classification algorithms for liver disease diagnosis, Int. J. Database Manage. Syst., vol. 3, no. 2, pp. 101–114, May 2011.
28. D. Dua and C. Graff, UCI Machine Learning Repository. Irvine, CA: University of California, School of Information and Computer Science, 2019.
29. F. Pedregosa, G. Varoquaux, A. Gramfort, V. Michel, B. Thirion, O. Grisel, M. Blondel, P. Prettenhofer, R. Weiss, V. Dubourg, J. Vanderplas, A. Passos, D. Cournapeau, M. Brucher, M. Perrot, and É. Duchesnay, Scikit-learn: Machine learning in Python, J. Mach. Learn. Res., vol. 12, pp. 2825–2830, 2011.
30. Y. Xu and R. Goodacre, On splitting training and validation set: A comparative study of cross-validation, bootstrap and systematic sampling for estimating the generalization performance of supervised learning, J. Anal. Test., vol. 2, no. 3, pp. 249–262, 2018.
31. R. Kohavi, A study of cross-validation and bootstrap for accuracy estimation and model selection, in Proc. 14th Int. Joint Conf. Artif. Intell. (IJCAI), vol. 2, 1995, pp. 1137–1143.
32. N. V. Chawla, K. W. Bowyer, L. O. Hall, and W. P. Kegelmeyer, SMOTE: Synthetic Minority Over-sampling Technique, J. Artif. Intell. Res., vol. 16, pp. 321–357, 2002, doi: 10.1613/jair.953.
33. A. Fernández, S. García, M. Galar, R. C. Prati, B. Krawczyk, and F. Herrera, Learning from Imbalanced Data Sets. Cham: Springer, 2018.
34. D. W. Hosmer, S. Lemeshow, and R. X. Sturdivant, Applied Logistic Regression, 3rd ed. Hoboken, NJ: John Wiley & Sons, 2013.
35. S. M. Lundberg and S.-I. Lee, A unified approach to interpreting model predictions, in Advances in Neural Information Processing Systems (NeurIPS), vol. 30, 2017, pp. 4765–4774.
36. M. T. Ribeiro, S. Singh, and C. Guestrin, "Why should I trust you?": Explaining the predictions of any classifier, in Proc. 22nd ACM SIGKDD Int. Conf. Knowl. Discovery Data Mining, 2016, pp. 1135–1144, doi: 10.1145/2939672.2939778.

